Theoret. chim. Acta (Berl.) 26, 107—130 (1972)

Molecular Orbital Calculations of the Active Site Complex of Two Iron Ferredoxins

II. Electron Distribution, Magnetic Moment, Field Gradients and Electronic Spectra of the Oxidized State

GILDA H. LOEW and DAVID A. STEINBERG
Department of Genetics, Stanford University Medical Center, Stanford, California 94305, USA

Received August 11, 1971/February 14, 1972

In this report we present further results of molecular orbital calculations for a model of the active site complex of two iron ferredoxins, using the Iterative Extended Hückel Method for our calculations. In the first paper of this series we dealt mainly with energy-conformation calculations which helped establish the salient chemical and conformational features of the lowest energy forms for such a complex. Presented here are the nature and energy ordering of the 70 molecular orbitals in the active site model, a calculation of room temperature magnetic moment, of the electric field gradient at the Fe nucleus and an assignment of the optical absorption spectra in the one electron approximation for the lowest energy conformer of the oxidized state of these proteins. For each property, we compare our calculated results with experiment whenever possible, and with the results of previous correlations. In addition, we indicate the sensitivity of these properties to variations in conformation about the Fe atoms.

In der vorliegenden Arbeit werden weitere Resultate der Untersuchung eines Modells des an der aktiven Stelle gebildeten Komplexes von zwei Eisen-ferredoxinen mitgeteilt, die mit Hilfe der iterativen erweiterten Hückel-Methode gewonnen wurden. In der ersten Veröffentlichung dieser Reihe wurden hauptsächlich die Ergebnisse der Berechnungen von Konformationsenergien angegeben, die dazu beitrugen, die wichtigsten chemischen Eigenschaften sowie die Konformationen solcher Komplexe mit der niedrigsten Energie zu ermitteln. Hier werden nun die Eigenschaften der 70 niedrigsten Molekülorbitale des Modells, eine Berechnung des magnetischen Moments bei Raumtemperatur und des elektrischen Feldgradienten am Fe-Kern sowie die Zuordnung des optischen Absorptionsspektrums in der Einelektronennäherung für die Konformation niedrigster Energie des oxydierten Zustandes dieser Proteine veröffentlicht. Die Ergebnisse werden soweit möglich mit dem Experiment und früheren Interpretationen verglichen. Zusätzlich wird auf die Empfindlichkeit dieser Eigenschaften bezüglich einer Variation der Konformation in der Nähe des Fe-Atoms hingewiesen.

1. Introduction and Background

The iron-sulfur proteins, now called "plant-type" ferredoxins, participate primarily as one-electron transfer agents in a wide variety of biological processes. Diverse biochemical and physical observations indicate that these proteins share a characteristic active site for electron transfer composed of two Fe atoms, two acid-labile S atoms of unknown origin, and four S atoms from nearby cysteine residues all in close proximity, as shown in Fig. 1 [1]. However, detailed chemical and conformational information about the active site is not known, nor are the variations from protein to protein in this class.

Presuming the biological activity to be centered on the two Fe atoms in the protein, a crystal field model of the active site as two Fe atoms perturbed by an

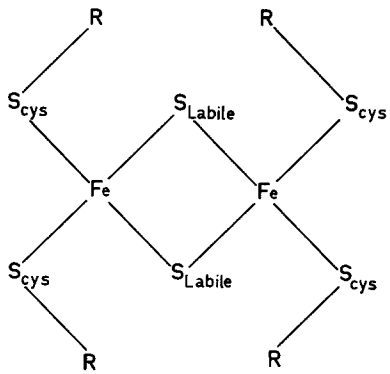

Fig. 1. General model of the active site of two-iron ferredoxins

electric field created by neighboring atoms [2–4], has been used in the past to try to understand some of its properties. In this crystal field approach the other atoms need not be specified and no interatomic interactions can be explicitly considered. Moreover even with these assumptions, no bona fide crystal field calculations characterizing these perturbed Fe ions have been made. Rather specific observations have been used to estimate further characteristics of the crystal field. Also for this reason and since there are important properties of these systems indicating interatomic interactions, we have undertaken a molecular orbital study of the active site which expands explicit consideration from two perturbed Fe ions to a molecular complex involving the core of atoms shown in Fig. 1.

The first step in our molecular orbital study was to select a reasonable model for the active site based on bona fide criteria. To this end, we have recently reported [5] the results of energy-conformation studies for a series of fifteen plausible active site models using the so-called Iterative Extended Hückel Theory (IEHT) for the molecular orbital calculations [6–12].

Previous applications of this method, including our own [9, 13, 14] indicate that such calculations yield total configuration energies whose variation with molecular geometry parallels that of the total energy and hence allows the prediction of a lowest energy conformation. The results of our calculations [5] showed persistent stability of a tetrahedral arrangement over a square planar one for all chemical variations studied of the oxidized state. In the lowest energy chemical-conformer, with RS^- in Fig. 1 = SCH_3^- each Fe has a distorted tetrahedral environment, the Fe–Fe distance is a maximum and the S_b–S_b distance is a minimum, typical of that of disulfide bonds in proteins. In the present study we use this most stable conformer to calculate the electric field gradient at the Fe nucleus, the room temperature paramagnetic susceptibility and to assign the optical spectra in the one-electron approximation of our calculations.

For each property discussed, our calculated results are compared with experimental results whenever possible and to previous explanations offered in the crystal field format. Since the conformer chosen is based on energy considerations only, agreement with observed properties is further independent verification

of the validity of the general nature of the active site complex which emerges from the molecular orbital description. In general, the satisfying result is obtained, that the lowest energy conformer is also the one which explains the observed properties most accurately and most consistently.

We proceed now to a general discussion of the nature of the molecular orbitals and energies which result from our calculations and then to a discussion of the three specific properties of the oxidized state mentioned above.

2. MO Results: Energy Ordering and Nature of the Molecular Orbitals

In our model for the oxidized state of the active site of the two-iron ferredoxins with $RS = SCH_3^-$ and no other added ligands, we have considered the four geometric variations shown in Fig. 2, and described in the table accompanying this figure, all of which have D_{2h} symmetry. As shown by the relative energies given in this table, the most stable conformer is IA_4. In these active site models there are 20 atoms, 70 valence atomic orbitals and 80 valence electrons which are all included in our IEHT calculation of the molecular orbital energies and eigen-

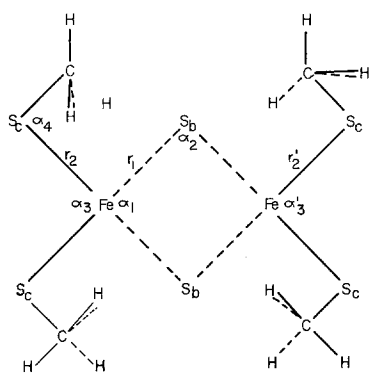

	A_1	A_2	A_4	A_5
α_1	109°	90°	45°	90°
α_2	71°	90°	135°	90°
α_3	109°	90°	109°	109°
α_4	90°	90°	90°	90°
r_1	2.32	2.32	2.42	2.32
r_2	2.32	2.32	2.32	2.32
r_2'	2.32	2.32	2.32	2.32
r(Fe-Fe)	2.66	3.26	4.20	3.26
$r(S_b-S_b)$	3.76	3.26	2.08	3.26
Energy	1151.7	1122.3	1163.7	1159.9

Fig. 2. Specific conformers of the active site: input geometries and calculated energies in eV

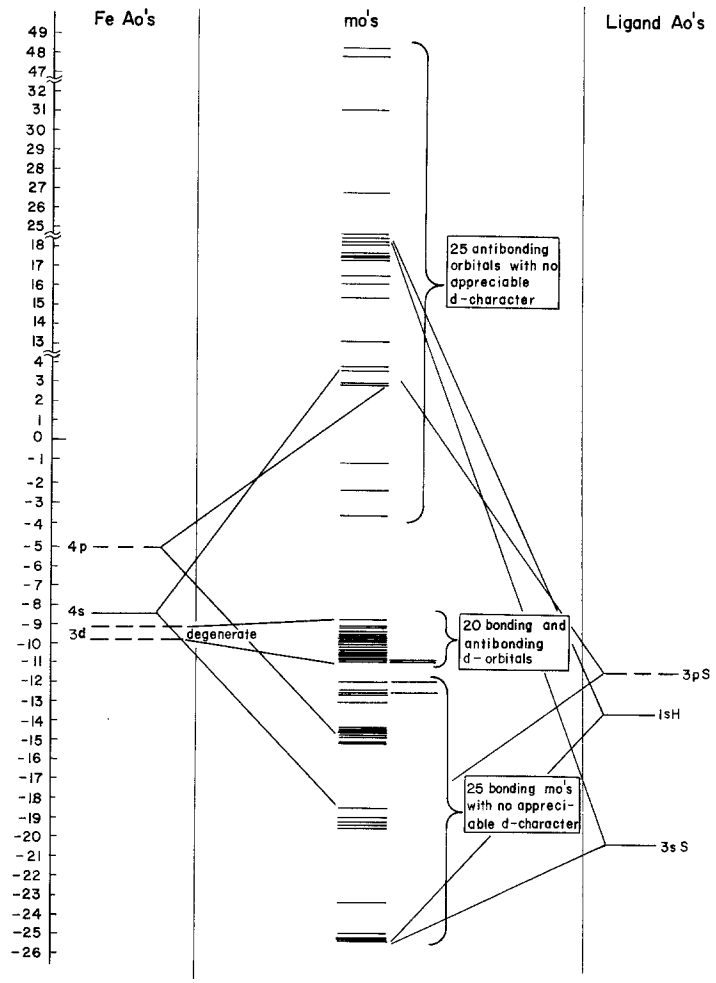

Fig. 3. Molecular orbital energy pattern for lowest energy conformer of the active site complex of two iron ferredoxins

functions. The resulting molecular orbital energy pattern is shown in Fig. 3 for the lowest energy conformer, together with the energy of the atomic orbitals and some indication of the nature of the molecular orbitals. While the details of this pattern depend on the molecular active site model chosen, the general features indicated are shared by all. In general then, there are a series of low lying bonding orbitals which involve no appreciable Fe 3*d* atomic orbitals. These result primarily from interactions among the ligand atoms themselves with some participation of the Fe 4*s* and 4*p* orbitals. In this model, the first 25 molecular orbitals are of this "perturbed ligand" type. These bonding orbitals have 25 anti-bonding partners of much higher energy (orbitals 46–70), also with no appreciable 3*d* orbital character. The energy difference between the highest filled bonding orbital and lowest empty non-bonding orbital of this type i.e.

$L \rightarrow L^*$ is 8.15 eV and is much too high an energy to be observed in UV or visible optical absorptions.

Between the 25 bonding and antibonding perturbed ligands and orbitals there are 20 very closely spaced energy levels. These are the energies of all the molecular orbitals which have appreciable 3*d* character. The first ten orbitals (26–35) have primarily sulfur (3*p*) ligand character, while the remaining ten (36–45) have primarily Fe 3*d* character, i.e. greater than 50% *d* orbital participation. These 20 orbitals correspond to the bonding and antibonding *d*-orbitals of the ligand field. However there is no large energy gap between these types of MO and the total energy separation among these 20 orbitals is only 1.85 eV or 15000 cm^{-1}. This value is much lower than that estimated from the crystal field formulation [2] and indicates weak-to-intermediate interaction of the 3*d* orbitals of Fe with the S ligands. The small perturbation of *d* orbitals by molecule formation can also be seen in Fig. 3 by noting the small energy difference between the 3*d* atomic and molecular orbitals. Perhaps this result of weak interaction which is the first attempt to characterize the bonding of Fe with S ligands, explains why the active site complex cannot be removed as an intact entity from these proteins in contrast to the heme group for which calculated metal-ligand interactions are much stronger [17, 18].

While the energies of the 20 molecular orbitals involving *d*-orbitals are closely spaced they are not pairwise degenerate and do not correspond to two separate Fe complexes. Moreover, the combination of AO's in these 20 orbitals is quite different from those in the two sets of ten orbitals that would be obtained from a ligand field description of two separated Fe atoms in tetrahedral symmetry. Each molecular orbital can be written as

$$\Psi_i(\Gamma_i) = \sum_{J=1}^{s} \alpha_{ij} A_{ij}(\Gamma_i) ,$$

where $\Psi_i = i^{\text{th}}$ MO belonging to irreducible representation Γ_i of D_{2h} symmetry group $A_J = J^{\text{th}}$ symmetry orbital of equivalent atoms A belonging to same irreducible representation

$$\text{A} = \text{Fe}, \text{S}_b, \text{S}_c, \text{C}_m, \text{H}_m, \text{H}'_m .$$

Table 1. Symmetry of binuclear *d* orbitals in D_{2h} symmetry

i	$d_{x^2-y^2}$	d_{z^2}	d_{xy}	d_{xz}	d_{yz}
$d_i + d_{i'}$	a_{1g}	a_{1g}	b_{1g}	b_{2g}	b_{3g}
$d_i - d_{i'}$	b_{3u}	b_{3u}	b_{2u}	b_{1u}	a_{1u}
T_D	e	e	t_2	t_2	t_2

In our active site complex there are six sets of symmetry equivalent atoms: The two Fe atoms, the two bridge S atoms (Sb), the four systeine S atoms (Sc), and four methyl carbon atoms (Cm), four of the methyl hydrogens which are in the plane of the major part of the molecule (Hm) and the 8 remaining methyl hydrogens which make up the tetrahedrally bonded carbon atoms (H′m). The ten 3*d* atomic orbitals participate in both the bonding and antibonding molecular orbitals as 10 binuclear pairs in the form: $(d_j \pm d'_j)$. Table 1 gives the irreducible

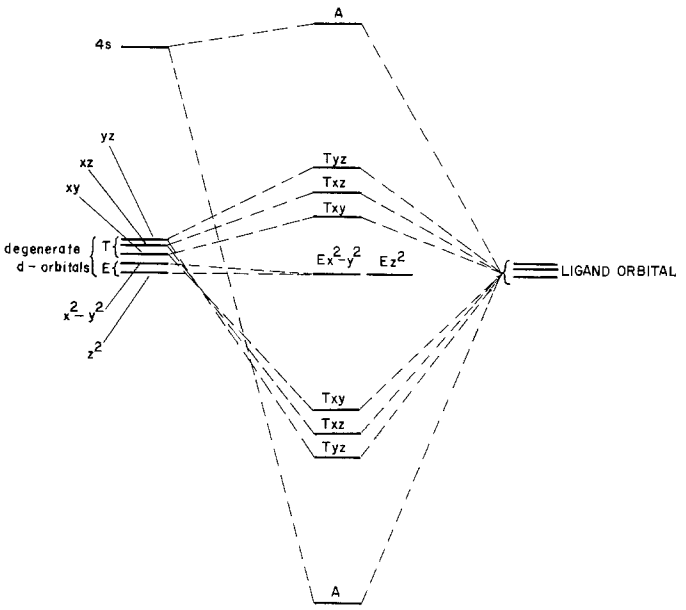

Fig. 4. Schematic ligand field bonding pattern for transition ion in T_d symmetry

representations to which the 10 combinations of d orbitals belong in the D_{2h} molecular symmetry. Also given for comparison in this table is the representations to which the individual d_j orbitals belong in the single centered Fe complexes of regular T_d symmetry.

We see that in the binuclear D_{2h} complex d orbitals can participate in MO's with both g and u symmetry.

A more detailed picture of the 10 antibonding, primarily d-orbitals so important in determining the observed properties is given in Fig. 5a for the lowest-energy active-site conformer. The symmetry labeling and % participation of the d orbitals in each molecular orbital is also given. These 10 states are shown separated into their g and u subsets. Each MO involves the participation of both Fe atoms. If the two parts of the binuclear complex were to separate and provided we supplied each Fe with its own bridge S atoms, which would involve an energy renormalization, this orbital diagram would approach two identical sets of 5 non-interacting, single $3d$ Fe molecular orbitals each with five electrons. The g or u subset alone of 5 antibonding primarily $3d$ orbitals correspond then to the five e^* and t_2^* orbitals shown in the Ballhausen type single metal ion in T_d symmetry diagram of Fig. 4 [16]. Contrary to the ligand field analysis of T_d symmetry, in which E orbitals are non-bonding, however, both the e^* and t_2^* orbitals contain some ligand character and both are separated in energy from their bonding partners.

The degree of interaction of the two Fe atoms can then be measured as the extent to which the g and u partners of the same d orbitals have different energies and different % covalences. We see from Fig. 5a that even with our lowest energy

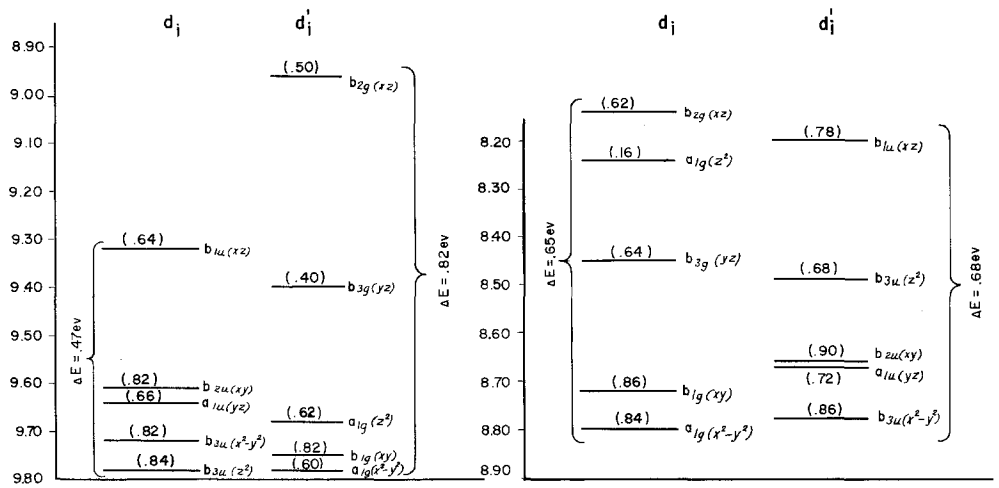

Fig. 5. Nature and energy ordering of the 10 antibonding d orbitals in active site complex of two iron ferredoxins. a tetrahedral conformation, b planar conformation of sulfur atoms about each Fe atom

conformer which involves a maximum Fe–Fe energy separation, this interaction is non-negligible on both criteria.

In the u-subset of molecular orbitals the two "e^*" ($d_{x^2-y^2}$ and d_{z^2}) orbitals are lower in energy than the three "t_2^*" orbitals and the partners of each type have non-degerate energies. For this series then the traditional energy interval called $10D_q = Et_2^* - E_e^* = 0.47\,\text{eV}\,(3800\,\text{cm}^{-1})$ analogous to the definition in single centered Fe complexes of regular T_d symmetry. For the g-subset we analogously define a second value of $10D_q$, as shown in Fig. 5, which is equal to 0.82 eV ($\sim 6500\,\text{cm}^{-1}$). These small values are similar to those empirically associated with four coordinated Fe T_d complexes [27b] and much less than values of 18000–36000 cm^{-1} previously proposed but not calculated for these ferredoxins [2, 3].

In Fig. 5b we give results obtained for a planar arrangement of all S atoms about each Fe atom. We see from this figure, that even though the Fe–Fe distance is smaller in this form, the effect of Fe–Fe interaction is somewhat less, and that the % of covalency and energy ordering of the various d orbitals is different in each case. The bonding MO's are also similarly rearranged.

In the ground state configuration, all of the 10 bonding orbitals and five of the ten antibonding orbitals shown in Fig. 5a involving 3d orbital character are completely filled. There are thus 5 primarily d electrons/Fe atom. In this respect then they resemble two formal Fe^{+3} ions. However, the MO occupancy is the result of our calculations and does not involve the preselection of the charge or the net spin on the Fe atoms or the specification of the number of 3d electrons. In fact, the total number of d electrons/Fe atom and the net charge on each which we calculate is quite different from the Fe^{+++} ion and resembles more closely a neutral Fe atom. This general result is shown in Table 2 and is true for all the chemical conformations studied independent of the formal charge on the Fe and ligand atoms.

Table 2. Net atomic charge and Fe valence electron density as a function of conformation

	q_{Fe}[a]	q_{sb}	q_{sc}	Z_{4s}[b]	Z_{4p_x}	Z_{4p_y}	Z_{4p_z}	$Z_{d_{x^2-y^2}}$	$Z_{d_{xy}}$	$Z_{d_{xz}}$	$Z_{d_{yz}}$	$Z_{d_{z^2}}$	$Z_t(d)$[c]	$Z_t(p)$	$Z_t(s)$
A_4	+0.10	−0.006	−0.102	0.44	0.23	0.16	0.18	1.97 (1.83)	1.18 (0.818)	0.85 (0)	0.88 (0)	1.99 (1.85)	6.87	0.57	0.44
A_5	0.14	−0.11	−0.08	0.52	0.21	0.34	0.24	1.82 (1.60)	1.01 (0.28)	1.40 (0.54)	1.40 (0.56)	0.92 (0.26)	6.65	0.79	0.52
A_1	+0.12	−0.13	−0.08	0.49	0.19	0.33	0.24	1.65 (1.36)	1.41 (0.46)	0.90 (0)	1.47 (0.98)	1.18 (0.46)	6.61	0.76	0.49
A_2	+0.02	+0.02	−0.20	0.40	0.22	0.18	0.14	1.86 (1.71)	2.00 (1.76)	1.35 (0.74)	0.57 (0)	1.15 (0.18)	7.03	0.54	0.40
Fe atm.[d]	0			2	0	0	0	1.2	1.2	1.2	1.2	1.2	6	0	2

[a] q_i = net charge on atom i.
[b] Z_i = electron density in Fe atomic orbital i.
[c] $Z_t(i)$ = total electron density in all Fe atomic orbitals of type i.
[d] Fe atom is the electron distribution in a neutral Fe atom.

Table 2 also gives the distribution of Fe valence electrons in the active site molecules for the four conformers studied. For comparison, the free atom configuration $(4s)^2(3d)^6(4p)^0$ is given with the six $3d$ electrons shown evenly distributed in the 5 degenerate d orbitals. For the lowest energy conformer A_4 each Fe has a total of $6.87(3d)$ electrons, $0.57(4p)$ electrons and $0.44(4s)$ electrons. Thus in their bonding the Fe atoms have donated a total of $1.56(4s)$ electrons to the ligands and in turn have received back $0.87(3d)$ and $0.57(4p)$ electrons resulting in a net forward donation of $+0.12e$ and the corresponding small positive charge on the Fe. In Table 2 is also indicated the total number of valence electrons in each Fe atomic orbital, and in parenthesis, the number of electrons in each atomic orbital involved in non-bonding orbitals. As seen, all of the $4s$ and $4p$ electron density is in bonding orbitals, since the corresponding antibonding orbitals are empty. However, the d electrons are involved in bonding to differing degrees. The strongest bonding orbitals are the d_{xz} and d_{yz} orbitals pointing more or less directly at the S ligands. These are 100% bonding. However only 7% of the $d_{x^2-y^2}$ and d_{z^2} and 31% of the d_{xy} electrons are involved. For the other conformers, we see that the net charge on each atom and in particular the distribution of the d electrons and the extent to which they are used in bonding varies even within a given symmetry type, i.e. different distorted T_D, and depends on the nature of the distortion. It is precisely the valence electron distribution together with the nature and energy of the molecular orbitals given in Figs. 3 and 5 which determine many properties of the complex such as the electric field gradient at the Fe nucleus as measured by the quadrupole splitting in Mössbauer resonance spectra of Fe^{57}. In the remainder of the paper then, we use the results just presented to calculate and discuss the magnetic moment, electric field gradient and electronic spectra of the oxidized active site for these two iron ferredoxins.

3. Magnetic Moment

It may be seen from Fig. 5 how we can explain the observed low temperature diamagnetism of the oxidized state of the two-iron ferredoxins directly from our molecular orbital results. It is simply that in the ground state configurations, the 5 lowest antibonding orbitals depicted are filled pairwise to give a diamagnetic state. As we indicated in our initial report [5], we have further confirmed this to be the lowest energy configuration by redoing the entire molecular orbital calculation for a number of biradical excited configurations in which an empty orbital is half filled by promotion of an electron from a totally paired orbital. On the other hand, for the two separate Fe^{+3} complexes which are used as the basis for the crystal field or ligand field models, there is no such natural way to obtain a totally diamagnetic state. Thus in the past [2–4] an antiferromagnetic exchange interaction has been invoked between the separated Fe^{+3} ions. However, no actual calculations of this interaction have been reported. Also, the temperature of $> 100°$ K at which appreciable paramagnetic susceptibility has been reported [19, 20] would correspond to an abnormally large exchange energy for such coupling.

Having obtained a diamagnetic ground state configuration we wished to make further use of our molecular orbital results by calculating a value for the room

temperature magnetic moment. The calculation of μ_{eff}^2 was carried out for all field independent terms, i.e. to second order. Since μ_{eff}^2 is a defined quantity given by:

$$\chi = \frac{N\beta^2}{3kT}\mu_{\text{eff}}^2 \,, \tag{1}$$

where χ is the magnetic susceptibility, the calculation must proceed through χ. Now χ is the magnetization per unit field strength, i.e.

$$\chi = M/H \tag{2}$$

and

$$\chi = \frac{M}{H} = \frac{N}{H}\frac{\sum\limits_N \mu_N e^{-E_N/kT}}{\sum\limits_N e^{-E_N/kT}} \,, \tag{3}$$

where $\mu_N =$ magnetic moment of state (N)

$$\mu_N = -\partial E/\partial H \tag{4}$$

$E_N =$ magnetic field energy of state (N).

To second order, the field independent value of χ is:

$$\chi = \frac{N\beta^2}{3kT}\Sigma N \frac{\left[\langle N/\boldsymbol{L}+\boldsymbol{2}S/N\rangle^2 + 2kT\sum\limits_M \frac{\langle N/\boldsymbol{L}+\boldsymbol{2}s/M\rangle\langle M/\boldsymbol{L}+\boldsymbol{2}S/N\rangle}{E_M - E_N}\right] e^{-\Delta E_N/kT}}{\sum\limits_N e^{-\Delta E_N/kT}} . \tag{5}$$

By comparing Eq. (1) and (5) we obtain a working definition of the effective magnetic moment to second order

$$\mu_{\text{eff}}^2 = \mu_x^2 + \mu_y^2 + \mu_z^2 = \mu_{\text{eff}}^2(1) + \mu_{\text{eff}}^2(2) , \tag{6}$$

$$\mu_{\text{eff}}^2(1) = \frac{\sum\limits_N \langle N/L + S/N\rangle^2 e^{-\Delta E_N/kT}}{\sum\limits_N e^{-\Delta E_N/kT}} , \tag{7}$$

$$\mu_{\text{eff}}^2(2) = 2kT\sum_N\sum_M \frac{\langle N/\boldsymbol{L}+\boldsymbol{2}S/M\rangle\langle M/L+2S/N\rangle}{E_M^0 - E_N^0} e^{-\Delta E_N/kT}/\Sigma e^{-\Delta E_N/kT} . \tag{8}$$

$\mu_{\text{eff}}^2(1)$ is the first order contribution of N electronic states to the effective magnetic moment. The sum over N is terminated when

$$\exp(-\Delta E_N^0/kT)$$

becomes negligible, i.e. $\leqq 0.01$. $\mu^2_{\text{eff}}(2)$ is the second order contribution of all states N due to their interactions with a series of states M. The sum over M is terminated when $(E^0_M - E^0_N)$ becomes large compared to the momentum interactions of the two states. χ will obey the Curie Law i.e., vary as $1/T$ only insofar as the ground state alone contributes to the magnetic moment, which is then T independent. Deviations from Curie Law behavior are then a sign that low lying excited states are contributing to the paramagnetic susceptibility. Since the angular momentum operator is a one-electron operator it can only connect configurations differing by one molecular orbital i.e. singly excited biradical states: $40 \rightarrow j$. Our calculations for the lowest energy conformer of the active site (A_4) indicate two such excited configurations might make a significant contribution to the room temperature susceptibility

$$\text{state (1)} \quad 40 \rightarrow 41 \quad \exp(-\Delta E_1/kT) = 0.23$$

$$\text{state (2)} \quad 40 \rightarrow 42 \quad \exp(-\Delta E_2/kT) = 0.05 \ ,$$

where ΔE_N in each case is the orbital promotion energy. Thus we include 3 product functions $\bar{\psi}_0, \bar{\psi}_1$, and ψ_2 in our calculations:

$$\begin{aligned} \bar{\psi}_0 &= \prod_L^{\text{val}} \ldots \phi_{40}\bar{\phi}_{40} = \cdots \phi_r \phi_s \, , \\ \bar{\psi}_1 &= \prod_L^{\text{val}} \ldots \phi_{40}\phi_{40} = \cdots \phi_r \phi_{s'} \, , \\ \psi &= \prod_L^{\text{val}} \ldots \phi_{40}\phi_{42} = \cdots \phi_r \phi_{s''} \, . \end{aligned} \tag{9}$$

Each molecular orbital is a linear combination of real atomic orbitals χ_i:

$$\phi_r = \sum_i C_{ri}\chi_i \tag{10}$$

and the molecular orbitals are ortho-normal.

Using such function for ψ_N, ϕ_r, and χ_i the first order orbital contribution to μ^2_{eff} is zero for each total state. The reason for this is as follows. For each state:

$$\langle N|L_i|N\rangle = \sum_i \sum_j C_{ri}C_{rj}\langle\chi_i|\boldsymbol{L}|\chi_j\rangle + \sum_l \sum_m C_{sl}C'_{sm}\langle\chi_l|\boldsymbol{L}|\chi_m\rangle \, . \tag{11}$$

Since the χ_i are real functions, they are not eigenfunctions of any component of $\boldsymbol{L}$. Thus there will be a first order orbital contribution only if the orbital momentum operator transforms one atomic orbital into another in the same orbital. This condition is not met for any molecular orbital then

$$\langle\phi_s|\boldsymbol{L}|\phi_{s'}\rangle = \langle\phi_r|\boldsymbol{L}|\phi_r\rangle = 0$$

Table 3. Matrix elements of spin operators for triplet state components

$S_l M_s$ / $S' M_s$	$\lvert 2S_z\rvert^2$				$(2S_x)^2$				$(2S_y)^2$			
	0, 0	1, 1	1, 0	1, −1	0, 0	1, 1	1, 0	1, −1	0, 0	1, 1	1, 0	1, −1
0, 0	0											
1, 1		4					2				2	
1, 0			0			2		2		2		2
1, −1				4			2				2	

and orbital angular momentum contribution is "quenched". To first order then there is only a spin contribution to μ_{eff}^2 and that only from the excited biradical states, since the ground state is totally spin paired.

Each excited configuration has the same orbital function but four possible spin states; three states with $S=1$, $M_s=1, 0, -1$ and a single state with $S=0$, $M_s=0$. Assuming equal weighting of the four states in the Boltzman averaging, the first order spin contribution of each configuration is a sum over four degenerate spin states q for each component of spin angular momentum S_i:

i.e. $$\langle N|2S_i|^2 N\rangle = \sum_{q',q}^{4} \langle N^q_{Sm_s}|2S_i|^2 N^{q'}_{S'm'_s}\rangle \; i=x,y,z\,.$$

For the $4|SM_s\rangle$ states possible from a biradical configuration, the non-zero matrix elements are given in Table 3. We see from this table that the 1st order spin contribution from both excited configurations are equal:

$$\sum_i \langle\psi_1|2S_i|^2\psi_1\rangle = \sum_i \langle\psi_2|2S_i|^2\psi_2\rangle = 3(8)\,.$$

The 2nd order contributions are of the form:

$$\langle N_{SM_s}|L+2S/M_{S'M'_s}\rangle\langle M_{S'M'_s}|L+2s|N_{Sm'_s}\rangle\,, \tag{12}$$

where states N and M differ by 1 orbital function. The spin operator does not alter the orbital function and all spin operator matrix elements are of the form:

$$\langle N|2S_i|M\rangle S_{rr'}S_{ss'}\,.$$

Since the molecular orbitals are orthogonal, $S'_{ii}=0$ and the second order spin contributions vanish.

For the orbital contribution; again because of orthogonality the only non-zero terms are of the form:

$$\langle\phi_s|L_i|\phi'_s\rangle = \sum_{j,k} c_{sj}c_{s'K}\langle\chi_j|L_i|\chi_K\rangle\,. \tag{13}$$

Table 4. Contributions[a] to $\mu_{eff}^2(300)$ in oxidized state of two-iron ferredoxins

$\langle N \vert$ \ $\vert M\rangle$	$\langle N\vert\mu_{eff}^2\vert M\rangle$		
	0[b]	1[b]	2[b]
0	0	0.62	0.82
1	0	5.52	0.04
2	0	−0.01	1.20

[a] Diagonal elements are 1st order contributions off-diagonal elements are 2nd order contributions.
[b] 0 = ground state contribution; 1, 2 = first and second excited state contribution.

To calculate these non-zero contributions, we make the approximation that the only significant contributions to L_i are from $3d$ atomic orbitals. Since the molecular orbitals ϕ_s which enter the calculation of magnetic moment are antibonding, nearly-pure d orbitals this is a reasonable simplification.

With these approximations then we have calculated the 1st and 2nd order contributions to $\mu_{eff}^2(300)$ from the ground and the first two excited state configurations. The individual terms in the numerators of Eqs. (7) and (8) are given in Table 4. To obtain μ_{eff}^2 these must be divided by

$$\sum_N \exp(-\Delta E_N^0/kT) = 1 + 4(0.23) + 4(0.05) = 2.16\,. \tag{14}$$

Then

$$\mu_{eff}^2 = [(1.44) + (5.56) + (1.19)]/2.16\,,$$

$$\mu_{eff}^2 = 8.19/2.16 = 3.78\,,$$

$$\mu_{eff} = 1.9\,BM/\mathrm{Fe}\,.$$

This result compares very favorably with Ehrenberg's measured room temperature value of $2.2\,BM$/Fe [21] and with the range of $1.3 - 2.2\,BM$ which have been reported elsewhere [19–21].

Thus both the low temperature diamagnetism and the room temperature paramagnetism can be quantitatively accounted for from our calculations. It is apparent that there is no need to invoke an exchange interaction between the two irons since the interaction is a natural product of electron delocalization in the molecule. Furthermore, the calculated value of the effective magnetic moment is in impressive agreement with experiments thus additionally eliminating the necessity of considering an anomalously energetic exchange interaction.

Field Gradient Calculation

Mössbauer Resonance studies of Fe^{57} substituted plant-type ferredoxins [15, 22] have made considerable contributions to the understanding of the nature

of the electron distribution about the two iron atoms. For example, recently it has been convincingly demonstrated [15] that two quadrupole doublets are present in the Mössbauer resonance spectra of the reduced ferredoxins indicating quite strongly the existence of two inequivalent iron sites in the reduced state. On the other hand, the oxidized state of seven different two-iron ferredoxins appear to have only one quadrupole split doublet and hence to have equivalent iron sites. From these experimentally derived results various explanations have been presented all within the crystal field framework. The concensus of opinion [2–4, 15] seems to favor a reduction scheme where one iron remains in the same oxidation state, ferric, while the other is reduced from ferric to ferrous. This model is proposed primarily on the basis that one of the quadrupole splittings in the reduced state has the same value as the oxidized state, a value of $\Delta E_Q \simeq +0.66$ mm/sec, while the second has a value of -2.63 mm/sec. In the crystal field format the smaller value is associated with a ferric ion and the larger value with a ferrous ion. Of course, in the molecular active site complex, it is naive to assume that any electron added will remain completely localized at one site of the molecule. Our preliminary results for one reduced site model [5], clearly show that both the added charge density and the spin density are distributed on all Fe and S atoms at the active site in agreement with observed hyperfine splitting of ESR spectra [29]. Because of the sensitivity of the electric field gradient (*efg*) to environment, as we shall indicate below, much smaller differences than gross spin or charge changes can account for large differences in electric field gradient and hence measured quadrupole splittings. It is unfortunate then that the physical data appears to corroborate in a superficial way the crystal field phenomenology which in turn is forced by the necessity of treating each iron atom separately. In any case, there has not been a calculation of the *efg* at the Fe^{57} nucleus in two-iron plant type ferredoxins. It was for these reasons then, that we chose to examine the problem from a molecular orbital viewpoint. The quadrupole Hamiltonian representing the interaction of the quadrupole moment with the electric field gradient can be written as follows:

$$\mathscr{H} = \frac{eQ}{4I(2I-1)} \{V_{zz}[3I_z^2 - I(I+1)] + (V_{xx} - V_{yy})(I_x^2 - I_y^2)\} , \tag{15}$$

where I is the nuclear spin vector, V_{xx}, V_{yy}, and V_{zz} are the principal axis components of the electric field gradient tensor, and Q is the quadrupole moment of the nucleus. By evaluating the matrix elements for the $I = 3/2$ state of the iron, the energy separation of the split states, ΔE_Q can be represented as

$$\Delta E_Q = \tfrac{1}{2} e^2 q Q [1 + \tfrac{1}{3} n^2]^{\frac{1}{2}} . \tag{16}$$

Where $q = V_{zz}/e$, $nq = (V_{xx} - V_{yy}/e)$ and = Quadrupole moment of $I = 3/2$ state, and the sign convention is such that for V_{zz} positive the $M_I = \pm 1/2$ state lies lowest.

It is this splitting ΔE_Q which is directly observed in Mössbauer Resonance spectra. Neither q, nq nor Q can be measured separately. Estimates of the quadru-

pole moment for the excited $I = 3/2$ nuclear state of Fe^{57} are available from Mössbauer resonance of other Fe containing complexes. Our object then was to calculate values of q and nq for various conformations of the ferredoxin active site including the lowest energy conformer to determine the sensitivity of electric field gradients to conformation about the Fe and also to determine if the calculated values of q and nq from our model of the active site were consistent with the measured values of ΔE_Q from Mössbauer resonance.

Since the electric field gradient operators are both one-electron operators and hence should yield reasonable expectation values with the product form for a total state function:

Since each MO is in turn a linear combination of atomic orbitals, the expectation value of the efg for each state is:

$$\langle \psi_N | eqg | \psi_N \rangle = \sum_{l}^{\text{a.o.}} \left[\sum_{j,l} C_{ij} C_{il} \langle \chi_i | eq f_{\text{Fe}} | \chi_j \rangle \right] , \tag{17}$$

where we use the term efg to mean either the q or nq operator. The coefficients C_{ij} of each atomic orbital in each molecular orbital are known as the result of our approximate solution of the Schroedinger equation. The matrix elements with the electric field gradient at the Fe nucleus are one, two and three-centered, one-electron integrals depending on the atoms to which the X_j and X_L orbitals belong. The 2 and 3 centered integrals, the "Lattice contributions" are attenuated in two ways from the one centered integrals or valence contributions. They are multiplied by a factor of $1/R^3$ where R is the distance from the ligand atom to the Fe nucleus and also by the overlap S_{jl} of the two atomic orbitals. Thus we consider them to be negligible compared to the valence contribution.

The total values of q and nq are then assumed to be the sum of the first order valence contribution of all electronic states of the molecule within thermal range of the ground state.

$$g_{\text{total}} = \frac{\sum_{N} \langle \psi_N | q | \psi_N \rangle \, e^{-\Delta E/kT}}{\sum e^{-\Delta E_N/kT}} , \tag{18}$$

$$(nq)_{\text{total}} = \frac{\sum_{N} \langle \psi_N | nq | \psi_N \rangle \, e^{-\Delta E_N/kT}}{\sum_{N} e^{-\Delta E_N/kT}} . \tag{19}$$

In the temperature range of 2.4–77° K for which the Mössbauer resonance spectra of the oxidized state of eight of the two-iron ferredoxins were obtained, no temperature dependence of the quadrupole splitting was observed [15]. In our lowest energy conformer, the first excited state is 0.04 eV above the ground state and ($\exp(-\Delta E/n \simeq 0.008)$). Hence, in agreement with observation, it would make a negligible contribution to the electric field gradient in the experimental temperature range. Thus we need only calculate the ground state contribution to the electric field gradients, i.e.

$$\langle \psi_0 | q | \psi_0^0 \rangle + \langle \psi_0 | nq | \psi_0 \rangle .$$

Table 5. Angular part of $\langle d_j | efg | d_l \rangle$ for $efg = q, \eta q$

χ_j	χ_l	q_{jl}	$(\eta q)_{jl}$
d_{xy}	d_{xy}	4/7	+3/7
d_{xz}	d_{xz}	−2/7	−3/7
d_{yz}	d_{yz}	−2/7	
$d_{x^2-y^2}$	$d_{x^2-y^2}$	−4/7	
d_{z^2}	d_{z^2}	+4/7	
p_z	p_z	+4/7	
p_x	p_x	+2/5	$-3\sqrt{10}/25$
p_y	p_y	+2/5	$+3\sqrt{10}/25$
$d_{x^2-y^2}$	d_{z^2}		$2\sqrt{3}/7$

The electric field gradient is a one electron operator centered on a specific atom and can be expressed as the product of a radial and an angular function which is a spherical harmonic $Y_l^m(\theta, \phi)$

$$\langle q \rangle = \langle V_{zz}/e \rangle = -\langle 3z^2 - r^2/r^5 \rangle = \langle 4\sqrt{\pi/5}\, Y_2^0(\theta, \phi)\, r^{-3} \rangle = Kqr^{-3}\, Y_2^0\,, \quad (20)$$

$$\langle nq \rangle = \left\langle \frac{V_{xx} - V_{yy}}{e} \right\rangle = -\left\langle \frac{3(x^2 - y^2)}{r^5} \right\rangle = -\langle 2\sqrt{6\pi/5}(Y_2^2 + Y_2^{-2})\, r^{-3} \rangle \quad (21)$$
$$= Knq\, r^{-3}(Y_2^2 + Y_2^{-2})\,.$$

Each atomic orbital is also the product of a radial and spherical harmonic function:

$$\chi = N_J R_J\, Y_J(\theta, \phi)\,. \quad (22)$$

Where N_J is a normalization constant.

Substituting expression (20), (21) and (22) into Eq. (17) for q and nq we have:

$$\langle \chi_J | q | \chi_L \rangle = \langle R_J | r^{-3} | R_L \rangle \langle Y_J | Y_2^0 | Y_L \rangle N_J N_L K_q \quad (23a)$$
$$= \langle R_J | r^{-3} | R_J \rangle\, q_{JL}$$
$$= \langle R_J | r^{-3} | R_L \rangle \langle Y_L | Y_2^2 + Y_2^{-2} | Y_L \rangle N_J N_L\, K_{nq} \quad (23b)$$
$$= \langle R_J | r^{-3} | R_L \rangle\, (nq)_{JL}\,.$$

Using these expressions then we have evaluated the angular portions of the one-electron, one-centered matrix elements of both the q and nq operators with the five ($3d$) and the three ($4p$) orbitals of the Fe atom. These matrix elements q_{JL} and $(nq)_{JL}$ are given in Table 5. It is interesting to note from this table that only diagonal elements in the atomic orbital basis set q_{JJ} contribute to the value of q while for nq there is one off-diagonal element $(nq)_{JL}$ between $d_{x^2-y^2}$ and d_{z^2}. There are then two "rhombic" corrections to the electric field gradient q; inequivalent diagonal contributions $(nq)_{JJ}$ from the two pairs of atomic orbitals d_{xz} and d_{yz} and p_x and p_y which cancel in axial symmetry and the cross term contribution between $d_{x^2-y^2}$ and d_{z^2} which is zero in axial symmetry.

Substitution the angular portions q_{jl} and nq_{jl} of the atomic Matrix elements into Eq. (17) we obtain for the angular part of the total ground state contribution:

$$q^{\text{val}} = \langle \psi_0 | q | \psi_0 \rangle = \sum_J^{\text{a.o.}} Z_J q_J \quad (24)$$

Table 6. Electric field gradient as a function of geometry in oxidized two-iron ferredoxins

	A_1	A_5	A_4	A_2
q^{val}	−0.119	−0.25	+0.151	+0.204
ηq^{val}	+0.30	+0.50	+0.064	+0.311
q_r^{val}	−0.204	−0.38	+0.151	+0.271

and for nq:

$$(nq)^{val} = \langle \psi_0(nq)\,\psi_0 \rangle = \sum_{J}^{a.o.} Z_J (nq)_J + 4 \sum_{i} C_{iJ} C_{il} (nq)_{Jl} \quad , \tag{25}$$

where Z_J = total electron density in atomic orbital,
C_{ij} = coefficient of the $d_{x^2-y^2}$ orbital in molecular orbital i,
C_{il} = coefficient of d_{z^2} orbital in molecular orbital i.
Assuming r^{-3} is the same for all atomic orbitals of Fe and using the antishielding factor $(1-R)$ to correct for polarization of core electrons the total contribution can be written in the form

$$q = (1-R)\langle r^{-3} \rangle\, q^{val}\,, \tag{26a}$$

$$nq = (1-R)\langle r^{-3} \rangle\, (nq)^{val}\,. \tag{26b}$$

Combining (26a) and (26b) we may further define the final rhombic-corrected "electric field gradient" as:

$$q_R^{val} = q^{val}\left(1 + \left[\frac{(nq)^{val}}{3(q)^{val}}\right]^{\frac{1}{2}}\right). \tag{27}$$

Then Eq. (16) becomes:

$$\Delta Eq(\text{mm/sec}) = 9.18\, Q(\text{barns})\,(1-R)\,\langle r^{-3} \rangle \text{ a.u. } q_R^{val}\left(\frac{esu}{cm^3}\right) \quad , \tag{28}$$

where the sign of q_R^{val} is determined by the sign of q^{val} and q^{val} is positive if the $M_I = \pm 1/2$ state lies lowest. From Eqs. (24) and (25) we see that the sensitivity of the electric field gradient and hence the observed quadrupole splitting to changes in the molecular environment about the Fe nuclei will be manifest primarily as changes in the electron density Z_J in the $4p$ and $3d$ orbitals of the Fe atoms. Substituting the values of Z_J listed in Table 2, the values of q_{jJ} and $(nq)_{JL}$ listed in Table 5, and the calculated values of C_{ij}, C_{il}, into Eq. (24), (25), and (27) we have calculated the values of q^{val}, $(nq)^{val}$ and q_R^{val} for the four conformers of the active site. These are given in Table 6. We see from this table that both the magnitude and sign of q^{val} and the magnitude of the $(nq)^{val}$ term are quite sensitive to the systematic small changes in geometry. Hence different values of electric field gradient are not necessarily an indication of gross difference in the nature of the Fe such as change in oxidation state or spin state or even of large conformation changes. It is interesting to note that the variation in q_R^{val} is greater within the 3 tetrahedral conformers than it is between tetrahedral and square planar conformation.

We obtain a minimum value of q_R^{val} for our lowest energy conformer. For this active site geometry moreover, q^{val} is positive and the value of η itself

$$\eta = \frac{(nq)^{val}}{q^{val}} = \frac{V_{xx} - V_{yy}}{V_{zz}} = 0.236 .$$

In the most recent Mössbauer resonance experiments reported [15] for seven ferredoxins all values of q were found to be positive and a value of η was reported which varied among the seven proteins from (0.05 ± 0.2) to (0.5 ± 0.2). Our calculated value of $\eta = 0.236$ then is not only well within the experimental range, it is a value which fits all of the observed values for the seven compounds. To compare our value of q_R^{val} with the quantity measured experimentally ΔE_Q we can use Eq. (28). Indirect experimental estimates of Q have yielded estimates varying from 0.187–0.47 Barns [23], with the lower end of this range favored. For the value of $(1-R) \cdot r^{-3}$ we have used 3.3 a.u. the results of the Freeman and Watson SCF calculation for Fe atom [24]. Using these values of $Q(I-R)(r^{-3})$ and our calculated value of q_R^{val} in Eq. (28) we obtain

$$\Delta E_Q = +0.91 \text{ mm/sec} .$$

This value while high is in remarkably good agreement with the experimental values of $+0.61$ to $+0.73$ (mm/sec) for the seven oxidized ferredoxins measured [15]. Hence the results of our molecular orbital calculations for a minimum energy conformer with equivalent Fe sites, gives the correct sign for ΔE_Q, corroborates its temperature independent magnitude in the range 4.2–77°, gives a value of η that agrees with all of the observed estimates, and finally gives reasonable numerical agreement with all of the measured values of ΔE_Q.

4. Optical Absorption Spectra

The optical absorption spectra of a number of two-iron ferredoxins, in particular spinach, putidaredoxin and adrenodoxin, have been obtained at low temperatures both in the oxidized and reduced state in the region of 2000–10000 Å by a number of investigators [25, 26]. More recent investigations have extended this region from 10000–25000 Å [27]. The spectra of different proteins are extremely similar and in general exhibit several poorly defined maxima even at low temperatures superimposed on a long-absorption tail. A composite spectra of the oxidized form of two of these proteins, putidaredoxin and spinach ferredoxin, from several experimental results is schematically presented in Fig. 6 in the well-studied region of 2000–10000 Å. Table 7 presents the assigned wave lengths of the absorption maxima including shoulders, with transition energies in eV and the molar extinction coefficient per Fe when experimentally available. We see from this table that the intensity of the absorption decreases gradually towards longer wave lengths from an ε of about 22000 at 2760 Å to 440 at 7000 Å. Recent work has also indicated the presence of a very weak transition at 6000 cm^{-1} [23].

Experimentally, the identification and assignment of these spectra has been quite difficult. Further insight into the nature of the electronic transitions comes

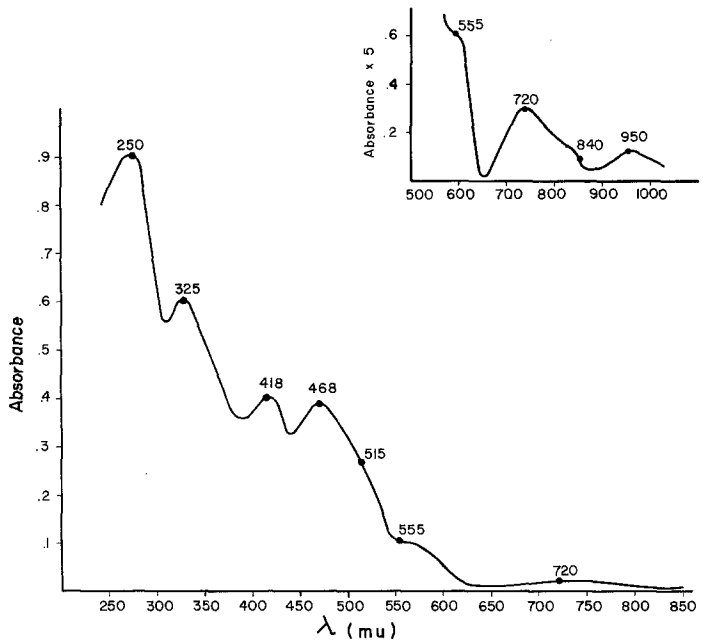

Fig. 6. Composite experimental spectra of two-iron ferredoxins in oxidized state

Table 7. Absorption maxima and shoulders of composite spectrum

λ(Å)	2760[a]	3250	4200	4680	(5150)[b]	7200	(8400)	9500
$\Delta E(cm^{-1})$	35200	307000	25000	213000	19400	14300	12000	10800
ΔE(eV)	4.4	3.8	2.9	2.63	2.4	1.8	1.5	1.3
E mmolar/Fe	10500	7000	5160	4650	3000	440	110	120

[a] From putidaredoxin spectrum.
[b] () means shoulder.

from the circular dichroism spectra of oxidized spinach and adrenodoxin [28]. The CD spectra in the region of 3000–7000 Å indicate that all the observed transitions are electric dipole allowed. Given the one-electron nature of our energy levels, i.e. the use of configuration rather than total state energies and the neglect of configuration interaction, we cannot hope for a quantitative one-to-one assignment of the spectra at this point. We reserve this task for a later study in which total state energies will be estimated. However it is possible to gain significant insight into three areas of much general interest. These are; (1) the nature of the transitions in the UV, visible, and IR; (2) a tentative identification of some observed transitions; (3) a theoretical rationale for continuous absorption of decreasing intensity from the UV to near IR. The general nature of the transitions can be seen by reference to Fig. 3. For example our results indicate that no observed transition is of the $L-L^*$ type, from a bonding to an antibonding perturbed-ligand orbital with no d character. The lowest of such transitions is 8.24 eV

(1500 Å) a higher energy than the limit of the observed UV region. Further reference to Fig. 3 shows that the entire observed spectra must be due to transitions between the closely spaced molecular orbitals 19–46, most of which contain some d orbital character. These are of three types in order of decreasing energy: $L \rightarrow d^*$, $d \rightarrow d^*$ and $d_i^* \rightarrow d_j^*$. The first two can be called charge transfer since they are from filled ligand bonding orbitals to empty-antibonding orbitals. Only the last type from filled to empty antibonding orbitals can be called $d \rightarrow d$ transitions where i = MO 36–40 and j = MO 41–45. Our results predict that these transitions would occur in the IR. At this point it is important to note that some $d \rightarrow d$ transitions can be electric dipole allowed since, as we have shown above, d orbitals participate in both g and u molecular orbitals in these binuclear D_{2h} complexes.

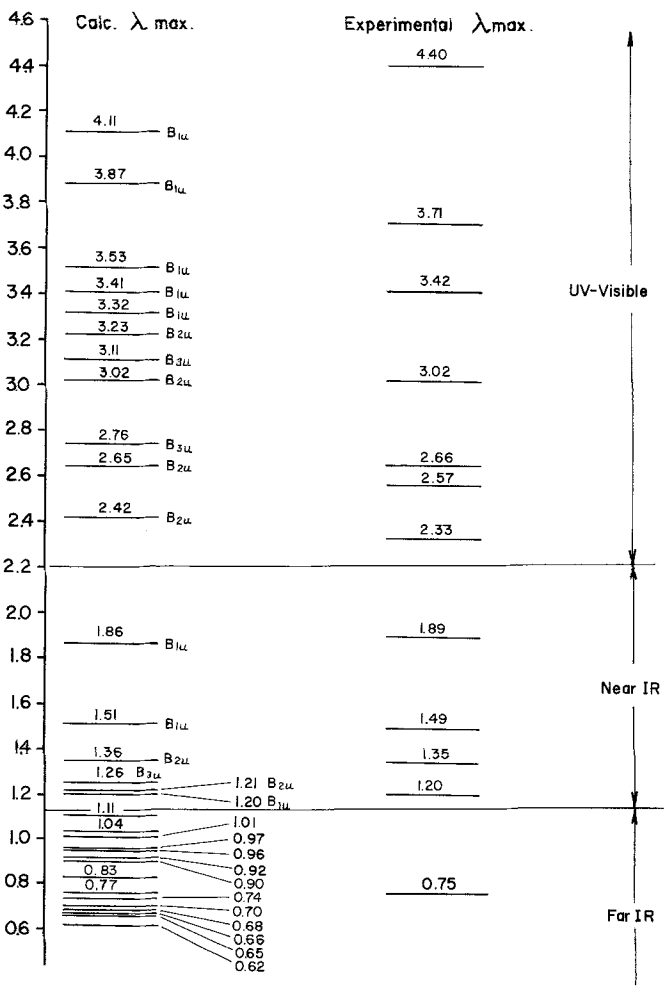

Fig. 7. Comparison of experimental and calculated values of absorption maxima for oxidized two-iron ferredoxin spectra

To further categorize and possibly assign the spectra, the symmetry-allowed electric dipole transitions were determined. The energy and symmetry of each of these are given in Fig. 7 together with the experimentally observed maxima. In Table 8a, b and c more detailed information is given for these transitions. They are divided into a) the well studied UV and visible region, b) the near IR region from 7000–10000 cm^{-1} and c) the newly explored far IR region below 10000 Å. In these tables are given along with the transition energy, the two orbitals involved in the transitions, the total symmetry of the excited state, the type of transition and the % d-character of the promoting orbital.

We see from Table 8a that all of the transition in the UV and visible are of the charge transfer type $L - d^*$, with about the same % d-character in each promoting orbital. From Fig. 7, we see that for each of the 7 observed peaks or shoulders in this region of the spectra there is a corresponding calculated value of transition energy. However there are four more symmetry allowed transitions calculated than peaks observed. These are bunched in the visible region between 3500 and 5500 Å. This density of states then can perhaps explain the almost continuous absorption and the lack of resolution of the individual transitions in this region.

Table 8a. UV-visible transitions

$(b \rightarrow d)$[a]	b[a]	ΔE	TSS[b]	Type	$f_d(L)$[c]
$(m \rightarrow 45)$	19	4.11	B_{1u}	$L \rightarrow d^*$	$0.14(x^2 - y^2, z^2)$
$(m \rightarrow 45)$	21	3.87	B_{1u}	$L \rightarrow d^*$	$0.10(x^2 - y^2, z^2)$
$(l \rightarrow 44)$	20	3.53	B_{1u}	$L \rightarrow d^*$	$0.12(x^2 - y^2, z^2)$
$(k \rightarrow 43)$	22	3.41	B_{1u}	$L \rightarrow d^*$	$0.11(xy)$
$(l \rightarrow 44)$	23	3.32	B_{1u}	$L \rightarrow d^*$	$0.09(x^2 - y^2, z^2)$
$(j \rightarrow 42)$	20	3.23	B_{2u}	$L \rightarrow d^*$	$0.12(x^2 - y^2, z^2)$
$(m \rightarrow 45)$	24	3.11	B_{3u}	$L \rightarrow d^*$	$0.09(xz)$
$(j \rightarrow 42)$	23	3.02	B_{2u}	$L \rightarrow d^*$	$0.09(x^2 - y^2, z^2)$
$(l \rightarrow 44)$	25	2.76	B_{3u}	$L \rightarrow d^*$	$0.07(xz)$
$(k \rightarrow 43)$	24	2.65	B_{2u}	$L \rightarrow d^*$	$0.09(xz)$
$(i \rightarrow 41)$	25	2.42	B_{2u}	$L \rightarrow d^*$	$0.07(xz)$

[a] b = promoting orbital, d = excited orbital.
[b] TSS = Total state symmetry.
[c] $f_d(L) = d$ electron density in the lower energy orbital.

Table 8b. Near IR transitions

$(b \rightarrow d)$	b	ΔE	TSS[a]	Type	$f_d(L)$
$(m \rightarrow 45)$	27	1.86	B_{1u}	$d \rightarrow d^*$	$0.29(x^2 - y^2, z^2)$
$(l \rightarrow 44)$	26	1.51	B_{1u}	$d \rightarrow d^*$	$0.31(x^2 - y^2, z^2)$
$(m \rightarrow 45)$	32	1.36	B_{2u}	$d_i^* \rightarrow d_j^*$	$0.41(yz)$
$(l \rightarrow 44)$	30	1.26	B_{3u}	$d_i^* \rightarrow d_j^*$	$0.45(xz)$
$(j \rightarrow 42)$	26	1.21	B_{2u}	$d \rightarrow d^*$	$0.31(x^2 - y^2, z^2)$
$(k \rightarrow 43)$	29	1.20	B_{1u}	$d \rightarrow d^*$	$0.26(xy)$

[a] TSS = Total state symmetry.

Table 8c. Far IR

$(b \rightarrow d)$[a]	b	ΔE	TSS[b]	Type	$f_d(L)$[c]
$(m \rightarrow 45)$	34	1.11	B_{3u}	$d_i^* \rightarrow d_j^*$	$0.40(xz)$
$(l \rightarrow 44)$	31	1.04	B_{2u}	$d_i^* \rightarrow d_j^*$	$0.47(yz)$
$(j \rightarrow 42)$	28	1.01	B_{3u}	$d \rightarrow d^*$	$0.29(xy)$
$(i \rightarrow 41)$	28	0.97	B_{1u}	$d \rightarrow d^*$	$0.29(xy)$
$(l \rightarrow 44)$	33	0.96	B_{2u}	$d \rightarrow d^*$	$0.10(yz)$
$(i \rightarrow 41)$	30	0.92	B_{2u}	$d_i^* \rightarrow d_j^*$	$0.44(xz)$
$(k \rightarrow 43)$	32	0.90	B_{3u}	$d_i^* \rightarrow d_j^*$	$0.41(yz)$
$(m \rightarrow 45)$	36	0.83	B_{1u}	$d_i^* \rightarrow d_j^*$	$0.86(x^2-y^2, z^2)$
$(m \rightarrow 45)$	39	0.77	B_{1u}	$d_i^* \rightarrow d_j^*$	$0.89(x^2-y^2, z^2)$
$(j \rightarrow 44)$	31	0.74	B_{1u}	$d_i^* \rightarrow d_j^*$	$0.47(yz)$
$(i \rightarrow 41)$	31	0.70	B_{3u}	$d_i^* \rightarrow d_j^*$	$0.47(yz)$

[a] b = promoting orbital, d = excited orbital.
[b] State TSS = Total state symmetry.
[c] f_d = Coefficient of d atomic orbital in molecular orbital b.

From Table 8b we see that the assignment in the near IR region below 7000 Å are characterized in our calculation by a significant increase in d character of the promoting orbital so that we can label most of the transitions in the near IR region $d \rightarrow d^*$ charge transfer transitions. In this region from 1.86–1.20 there is an almost 1 for 1 assignment of observed and calculated absorption maxima and shoulders possible. Three different excited states are almost superimposed at 10000 Å, and three other calculated transitions correspond almost exactly to the other three higher energy transitions.

Below 10000 Å we see from Table 8c and from Fig. 7 that there are a large number of closely spaced, symmetry-permitted transitions. All but 3 of these 11 states are $d_i^* \rightarrow d_j^*$ transitions from filled to empty antibonding d orbitals. There is then another marked increase in the % d character in the promoting orbital in going from the near to far IR. While the experimental results are not yet definitive it appears that there is only one observed transition in this region at about 0.75 eV. Having indicated the nature of the UV, visible, and the transitions, and examined some of the specific maxima involved, we turn to a discussion of the relative absorption intensities observed in the different wave length regions.

Transition moments, are often assumed to be proportional to the overlap of the atomic orbitals in the two molecular orbitals involved in the transition. Since the two Fe atoms are fairly far apart in this model, the overlap of the two centered d orbitals is very small i.e. $\langle d_i | d_j' \rangle = 0.04$ while the one-centered $3d$ overlaps are exactly zero. Thus while $d_i^* \rightarrow d_j^*$ transitions are not strictly symmetry forbidden, they are likely to be very weak. With this reasoning then, since then overlap of orbitals between the Fe and S ligands is much greater than on the two Fe atoms, and since all the excited orbitals are antibonding primarily d orbitals, the more ligand character in the promoting orbitals i.e. the greater the intensity would be, i.e. $I(L \rightarrow d_i^*)\, I(d \rightarrow d^*)\, I(d_i^* \rightarrow d_j^*)$. The elimination of the $L \rightarrow L^*$ transition by energy consideration explains the lower observed intensity of the UV spectra for ferredoxins than for one iron complexes such as hemes, and at the same time explains why the UV and visible transitions which are all of the $L \rightarrow d^*$

type with very little d character in the bonding orbitals are the most intense in this protein. We would also predict a sharp decrease in intensity between the transition at 2.42 eV (about 5100 Å) and the one at 1.86 eV (7200 Å) and in general between the invisible and IR spectra which are mainly $d \rightarrow d^*$. This result is in agreement with the observed order of magnitude decrease in intensity indicated in Table 7. If the intensity is decreased another order of magnitude or more by the increase in d character in the antibonding over the bonding d orbitals i.e. in $d_i^* \rightarrow d_j^*$ over $d_i \rightarrow d^*$ it is then understandable why no measurable for IR absorption is obtained. The exception would be the $L \rightarrow d^*$ transition at 0.96 eV. This then may correspond to the one observed transition maximum at 6000 cm^{-1} seen in this region [23].

To summarize then, our one-electron approximation to the assignment of the optical spectra of the oxidized ferredoxins, we have tentatively identified the type of absorptions involved in the UV, visible, near IR and far IR regions, accounted for their diminishing intensity and for the regions of continuous absorption. We have also made some actual numerical correspondence between calculated and observed transition maxima. Further elucidation of these spectra await our two-electron and configuration-interaction corrections and a more quantitative estimate of relative oscillator strengths of the different allowed transitions.

Acknowledgement. The authors wish to gratefully acknowledge sponsorship of NSF Grant GB 17980.

Bibliography

1. Tsibris, J.C.M., Woody, R.W.: Coordin. chem. Rev. **5**, 417 (1970).
2. Brintzinger, H., Palmer, C., Sands, R.H.: Biochem. **55**, 397 (1966).
3. Gibson, J.F., Hall, D.O., Thornley, T.H.M., Whatley, F.R.: Proc. nat. Acad. Sci. USA **56**, 987 (1966).
4. Thornley, J.H.M., Gibson, J.F., Whatley, F.R., Hall, D.O.: Biochem. biophysic. Res. Commun. **24**, 877 (1966).
5. Loew, G., Steinberg, D.: Theoret. chim. Acta (Berl.) **23**, 239 (1971).
6. Rein, R., Fukuda, N., Win, H., Clarke, G.A., Harris, F.E.: J. chem. Physics **45**, 4743 (1966).
7. Zerner, M., Gouterman, M.: Theoret. chim. Acta (Berl.) **4**, 44 (1966).
8a. Hoffman, R.: J. chem. Physics **39**, 1397 (1963).
8b. — J. chem. Physics **40**, 2480 (1964).
9. Hoyland, J.R.: Semiemperical MO theories: A critique and a review of progress.
10. Zerner, M., Gouterman, M., Kobayashi, H.: Theoret. chim. Acta (Berl.) **6**, 363 (1966).
11. Pullman, A., Pullman, B.: Progress in Nucleic Acid Research and Molecular Biology **9**, 327 (1969).
12. Wolfberg, M., Helmholtz, L.: J. chem. Physics **20**, 837 (1952).
13a. Pan, D.C., Allen, L.C.: J. chem. Physics **46**, 1797 (1967).
13b. Allen, L.C., Russell, J.D.: J. chem. Physics **46**, 1029 (1967).
14. Loew, Gilda: Theoret. chim. Acta (Berl.) **20**, 203 (1971).
15. Bearden, A.J., Dunham, W.R.: Structure and Bonding **8**, 1 (1970).
16. Ballhausen, C.J.: Introduction to ligand field theory. San Francisco: McGraw-Hill 1970.
17a. Harris, G.: Theoret. chim. Acta (Berl.) **10**, 119 (1968).
17b. Harris-Loew, G.: Theoret. chim. Acta (Berl.) **17**, 18 (1970).
18. Gouterman, M.: J. molecular Spectroscopy **6**, 138 (1961).
19. Palmer, G.: Private communication, Sept. 1970.
20. Moss, T.H., Petering, D., Palmer, G.: J. biol. Chemistry **244**, 2275 (1969).
21. Ehrenberg, A.: Private communication, Aug. 1966.
22. Johnson, B.D., Bray, R.C., Commeda, R., Hall, D.O.: Proc. nat. Acad. Sci. USA **63**, 1234 (1969).
23. Harris, G.M., Weissbluth, M.: Physic. Rev. **149**, 198 (1966).
24. Freeman, A.J., Watson, R.E.: Physic. Rev. **131**, 2566 (1963).
25. Woody, R.W., Tsibris, J.C.M., Gunsalus, I.C.: Private communication.

26. Wilson, D. F.: Arch. Biochem. Biophysics **122**, 254 (1967).
27a. Palmer, G.: Private communication, Jan. 1971.
27b. Eaton, W.: Private communication, June 1971.
28. Palmer, C., Brintzinger, H., Estabrook, R. W.: Biochem. **6**, 1658 (1967).
29. Orme-Johnson, W. H., Beinert, H.: Ann. New York Acad. Sci. **158**, 336 (1968).

Dr. G. H. Loew
Departments of Genetics
Stanford University Medical Center
Stanford, California 94304, USA